NEOPLASIA
www.neoplasia.com

Volume 15 Number 11 November 2013 pp. 1272–1281 1272

Cyclin G2 Promotes Hypoxia-Driven Local Invasion of Glioblastoma by Orchestrating Cytoskeletal Dynamics[1,2]

Atsushi Fujimura*,†, Hiroyuki Michiue*, Yan Cheng*, Atsuhito Uneda*, Yasunari Tani*, Tei-ichi Nishiki*, Tomotsugu Ichikawa‡, Fan-Yan Wei§, Kazuhito Tomizawa§ and Hideki Matsui*

*Department of Physiology, Okayama University Graduate School of Medicine, Dentistry and Pharmaceutical Sciences, Okayama, Japan; †Advanced Research Training Program, Okayama University Graduate School of Medicine, Dentistry and Pharmaceutical Sciences, Okayama, Japan; ‡Department of Neurosurgery, Okayama University Hospital, Okayama, Japan; §Department of Molecular Physiology, Faculty of Life Sciences, Kumamoto University, Kumamoto, Japan

Abstract

Microenvironmental conditions such as hypoxia potentiate the local invasion of malignant tumors including glioblastomas by modulating signal transduction and protein modification, yet the mechanism by which hypoxia controls cytoskeletal dynamics to promote the local invasion is not well defined. Here, we show that cyclin G2 plays pivotal roles in the cytoskeletal dynamics in hypoxia-driven invasion by glioblastoma cells. Cyclin G2 is a hypoxia-induced and cytoskeleton-associated protein and is required for glioblastoma expansion. Mechanistically, cyclin G2 recruits cortactin to the juxtamembrane through its SH3 domain–binding motif and consequently promotes the restricted tyrosine phosphorylation of cortactin in concert with src. Moreover, cyclin G2 interacts with filamentous actin to facilitate the formation of membrane ruffles. In primary glioblastoma, cyclin G2 is abundantly expressed in severely hypoxic regions such as pseudopalisades, which consist of actively migrating glioma cells. Furthermore, we show the effectiveness of dasatinib against hypoxia-driven, cyclin G2–involved invasion *in vitro* and *in vivo*. Our findings elucidate the mechanism of cytoskeletal regulation by which severe hypoxia promotes the local invasion and may provide a therapeutic target in glioblastoma.

Neoplasia (2013) 15, 1272–1281

Introduction

Glioblastoma multiforme (GBM), the most common and malignant primary tumor arising in the central nervous system, is characterized by a variety of pathologic findings including vascular proliferation, aggressive invasion, and pseudopalisades [1], which are promoted by hypoxic conditions [2,3]. Pseudopalisades consist of necrotic foci and surrounding glioma cells and are a specific finding that distinguishes GBM from lower grade astrocytomas [4]. They were also shown to consist of hypoxic and actively migrating glioma cells [5].

In the expansion of GBM, hypoxia contributes to the maintenance of glioma stem cells, angiogenesis, and cellular migration through the accumulation of hypoxia-inducible factor 1α (HIF-1α) and consequent activation of several genes [6–8]. Studies using microarray-based gene expression profiling in glioma or neuroblastoma cells have

Address all correspondence to: Dr Hiroyuki Michiue, MD, PhD, 2-5-1 Shikata-cho, Kita-ku, Okayama City, Okayama Prefecture, Japan. E-mail: hmichiue@md.okayama-u.ac.jp

[1]This work is supported by a Grant-in-aid for Scientific Research from the Ministry of Education, Science, Sports and Culture of Japan, by Okinaka Memorial Institute for Medical Research, and by a Grant-in-aid for Scientific Research from the Ministry of Health, Labor and Welfare of Japan. A.F. is supported by the Advanced Research Training Program (Okayama University Hospital) and Sekizenkai, a foundation of Okayama University Hospital. The authors declare no competing financial interests.
[2]This article refers to supplementary materials, which are designated by Figures W1 to W8 and are available online at www.neoplasia.com.
Received 7 August 2013; Revised 21 October 2013; Accepted 21 October 2013

DOI 10.1593/neo.131440

indicated the knockdown of HIF-1α to result in reduced expression of *ccng2* mRNA (which encodes cyclin G2), suggesting that cyclin G2 expression is hypoxia-responsive [9–11]. Cyclin G2 was first identified as a negative regulator of cell cycle progression [12] and shown to bind to an active complex of protein phosphatase 2A (PP2A) and induce a p53-dependent cell cycle arrest [13]. Moreover, cyclin G2 interacts with and stabilizes microtubules, suggesting that cyclin G2 contributes to the regulation of cytoskeletal dynamics [13]. Despite evidence that the expression and subcellular distribution of cyclin G2 were related to epithelial cancer progression and metastasis [14–16], the precise mechanism by which cyclin G2 controls tumor expansion is unclear, especially in GBM.

Although several studies have shown that hypoxia induced by tumor enlargement or antiangiogenic therapy stimulated the local invasion of glioblastoma cells by modulating signal transduction [8], we do not have sufficient evidence that hypoxia regulates cytoskeletal dynamics, which is required for cellular motility, to promote the local invasion of glioblastoma. Accordingly, the aim of this study is to elucidate the precise mechanism of cytoskeletal regulation in the hypoxia-driven invasion and thereby provide evidence of a therapeutic strategy in glioblastoma. Especially, we here focus on the roles of cyclin G2 in cellular migration in response to hypoxia from the viewpoint of cytoskeletal regulation.

Materials and Methods

Cell Culture and Reagents

Human glioma cell lines U87MG, U251MG, and LNZ308 and human embryonic kidney (HEK) 293 cells were cultured in Dulbecco's modified Eagle's medium (DMEM) with 10% FBS and penicillin/streptomycin (Life Technologies, Carlsbad, CA). Murine glioma-initiating 005 cells were cultured as previously reported [17]. For hypoxic stimulation, cells were cultured in medium containing 100 μM deferoxamine mesylate (Sigma-Aldrich, St Louis, MO) or hypoxic chamber maintained at 5% or 1% O_2. For the analysis of tyrosine phosphorylation, 10 μM erlotinib (LKT Laboratories, Inc, St Paul, MN) or 1 μM dasatinib (Selleck Chemicals, Houston, TX) was added before the hypoxic stimulation (Figure W7).

For the immunoblot analysis, the following antibodies were used as the primary antibody: anti–cyclin G2, anti-Src, anti-p21, anti-p53, anti-green fluorescent protein (GFP; Santa Cruz Biotechnology, Inc, Dallas, TX), anti–HIF-1α (Novus Biologicals, LLC, Littleton, CO), anti–α-tubulin, anti–β-actin (Sigma-Aldrich), anti-cortactin, anti-phosphotyrosine (Millipore, Billerica, MA), and anti-Src (Cell Signaling Technology, Inc, Danvers, MA). For the immunohistochemistry and immunofluorescence, the following antibodies were used: anti–cyclin G2, anti-Src, anti-CD68 (Santa Cruz Biotechnology, Inc), anti–HIF-1α (Novus Biologicals, LLC), anti-human glial fibrillary acidic protein (GFAP), anti-cortactin (Abcam, Cambridge, United Kingdom), anti–α-tubulin (Sigma-Aldrich), anti-cortactin, anti-phosphotyrosine (Millipore), and anti–phospho-Src (Y417) (Life Technologies). Alexa Fluor 555–conjugated phalloidin and Hoechst (Life Technologies) were used for the detection of F-actin and nuclei, respectively. Validation of the use of the cyclin G2 antibody in immunoblot, immunofluorescent, and immunostaining analyses was reported in the past studies [14,18,19] and was further confirmed as shown in Figure W7.

For the analysis of cell proliferation and viability, the water soluble tetrazolium-1 (WST-1) assay was performed according to the manufacturer's protocol (Roche, Tokyo, Japan).

Luciferase Reporter Assay

The human cyclin G2 promoter region (−1600∼0) was amplified from genomic DNA of U87MG cells and cloned into a pGL4.14 luciferase reporter vector (Promega, Madison, WI). The vectors were transfected into U87MG cells before hypoxic stimulation and cultured in a hypoxic chamber for 24 hours. The cells were lysed and incubated with the Luciferase Assay System (Promega) before measurements were made. Oligonucleotides for amplification of human cyclin G2 promoter region were given as follows: forward, 5′-CAAAACCCTCACCAAGCTCACACCTCTCTG-3′; reverse, 5′-CCCCTTGTTTTTGTTAAGAGTTTCGACGCC-3′.

Wound-Healing Assay

Cells were plated on Matrigel-coated glass slips at 90% confluence and cultured for 24 hours in DMEM with 10% FBS. The next day, the slips were scratched with white tips (200 μl), and the medium was switched to DMEM with 0.1% FBS. Then, the cells were incubated in normoxic or hypoxic conditions for 24 hours and observed. To examine the effects of ectopic expression of cyclin G2 on cellular motility, plasmids encoding cyclin G2–enhanced green fluorescent protein (EGFP), EGFP, $G2^{K219Q}$-EGFP, or $G2^{P291A}$-EGFP were transfected before the scratching.

Plasmids, Small Interfering RNA, and Retroviruses

The human cyclin G2 cDNA was purchased from OriGene (Rockville, MD; Cat. No. SC117452), and the open reading frame was cloned into a pEGFP-N3 (Clontech, Mountain View, CA) or a pcDNA3.1/V5-His TOPO vector (Life Technologies). The K219Q and P291A mutants were generated using the site-directed mutagenesis kit (Stratagene, La Jolla, CA). Small interfering RNA (siRNA) and scrambled RNA were obtained from Thermo Fisher Scientific Inc (Waltham, MA; Dharmacon, ON-TARGET*plus* siRNA Reagents). The retrovirus encoding scrambled shRNA or shRNA against human *ccng2* was prepared using the HuSH-29 plasmids (OriGene) and PT67 cells (Clontech) according to the manufacturer's recommendation.

RNA Purification, cDNA Synthesis, and Real-Time Reverse Transcription–Polymerase Chain Reaction

For reverse transcription–polymerase chain reaction (PCR) analysis, total RNA was isolated from GBM and cancer cells using an RNeasy kit (Qiagen, Santa Clarita, CA) and subjected to on-column digestion of genomic DNA with RNase-free DNase (TaKaRa, Otsu, Japan). With 1 μg of purified total RNA, cDNA was synthesized using a Maxima cDNA synthesis kit (Thermo Fisher Scientific Inc) Quantitative analyses of *CCNG2*, *FYN*, *CSK*, *SRC*, *LYN*, and *LCK* mRNA were performed with RT^2 SYBR Green master mixes (Qiagen) and the ABI PRISM 7000 Sequence Detection System (Life Technologies). As an internal control, the copy number of *ACTB* (β-actin) mRNA was determined. We obtained predesigned and certified primers from TaKaRa. All data were analyzed using software (7000v1.1; Life Technologies).

Western Blot Analysis and Preparation of Cytoskeletal Pellets

Immunoblot analysis was performed as described previously [20]. Cells were lysed in cell lysis buffer [20 mM Tris-HCl (pH 7.5), 150 mM NaCl, 1 mM EDTA, 1 mM EGTA, and 0.5% Triton X-100) containing Complete Proteinase Inhibitor Cocktail (Roche). For the detection of phosphoprotein, PhosSTOP Phosphatase Inhibitor Cocktail (Roche)

was added. Samples were subjected to sodium dodecyl sulfate (SDS)–polyacrylamide gel electrophoresis, blotted on a nitrocellulose membrane, and subjected to immunodetection. HRP signals were visualized using Chemiluminescent Peroxidase Substrates (Sigma-Aldrich) and detected by VersaDoc (Bio-Rad, Hercules, CA). Signal density was analyzed using the VersaDoc software. All raw data are shown in Figure W8.

For preparing a cytoskeletal fraction mainly containing filamentous actin, we used a G-actin/F-actin *In Vivo* Assay Biochem Kit (Cytoskeleton, Inc) with minor modifications. Briefly, EGFP-, cyclin G2–EGFP–, or $G2^{K219Q}$-EGFP–transfected U87MG cells were incubated with phalloidin (1 μg/ml) and nocodazole (200 ng/ml) for 2 hours before the fractionation of filamentous actin with the kit. For the microtubule pellet, the cells were incubated with latrunculin B (250 ng/ml) and paclitaxel (500 ng/ml) for 2 hours and lysed with microtubule stabilization buffer [50 mM Pipes (pH 6.9), 5 mM $MgCl_2$, 2 mM EGTA, 0.1% Triton X-100, 0.1% NP-40, 100 μM GTP, 1 mM ATP, 250 ng/ml latrunculin B, 500 ng/ml paclitaxel] before fractionation by ultracentrifuge (100,000*g*).

Immunohistochemistry and Immunofluorescence

Paraffin-embedded human GBM specimens were prepared in the Okayama University Hospital's Department of Pathology. Sections were deparaffinized, epitope-retrieved with proteinase XXV (Thermo Scientific), and blocked with 5% donkey serum in phosphate-buffered saline (Abcam). Slides were incubated at 4°C for 16 hours with primary antibodies, visualized with the ImmPRESS polymerized enzyme staining kit (VECTOR Laboratories, Burlingame, CA), and counterstained with hematoxylin. For the immunofluorescent analysis of human GBM specimens, sections were prepared as described above except for the secondary antibodies (Life Technologies; Alexa Fluor 488– or Alexa Fluor 555–conjugated antibodies). For the immunofluorescent analyses of glioma cell lines, cells were fixed with 4% paraformaldehyde (PFA) for 15 minutes, permeated with 0.2% Triton X-100 for 10 minutes, and blocked with 5% goat (Abcam) or donkey serum. The samples were then incubated with primary antibodies and secondary antibodies. Immunofluorescent samples were observed with a confocal laser scanning microscope (FluoView 300; Olympus, Tokyo, Japan).

Immunoprecipitation and Chromatin Immunoprecipitation Assay

To investigate the interaction between cyclin G2, cortactin, and src family kinases (SFKs), plasmids encoding EGFP, EGFP-tagged cyclin G2, or the EGFP-tagged cyclin G2 mutant were transfected into U87MG cells using Lipofectamine 2000 according to the manufacturer's instructions (Life Technologies). After 20 hours, cells were lysed with immunoprecipitation (IP) buffer [20 mM Tris-HCl (pH 7.5), 150 mM NaCl, 1% Triton X-100, and proteinase inhibitor cocktail] and centrifuged. The supernatant was precleaned with protein G sepharose, incubated with anti-GFP antibody, and precipitated with protein G sepharose. Precipitated samples were boiled in 2× SDS buffer. For detection of phosphotyrosine, hypoxia-stimulated or cyclin G2–transfected U87MG cells were lysed in IP buffer containing PhosSTOP (Roche) and immunoprecipitated with anti-cortactin antibody.

For chromatin immunoprecipitation (ChIP) assay, 5×10^7 U87MG cells (cultured in normoxic or hypoxic conditions for 24 hours) were incubated with formaldehyde (final concentration of 0.75%) at room temperature for 15 minutes and lysed with lysis buffer [50 mM Hepes (pH 7.5), 140 mM NaCl, 1 mM EDTA, 1% Triton X-100, 0.1% sodium deoxycholate, 0.1% SDS, protease inhibitor]. After sonication, DNA concentrations of the samples were determined and the samples containing 25 μg of DNA were immunoprecipitated with anti–HIF1-α antibody or control mouse IgG, followed by PCR. Oligonucleotides for the ChIP assay were given as follows: HIF-1α—forward, 5′-CTCT-TCCCAGGGACTATCTG-3′; reverse, 5′-GACTGAAGGAGG-GGCTTTTC-3′.

Statistical Analysis

Data were analyzed either by Student's *t* test to identify significant differences between two groups or by Scheffe's posttest following a two-way analysis of variance to compare multiple groups. *P* values less than .05 were considered significant.

Results

Cyclin G2: A Marker of Pseudopalisades

To unveil the mechanism by which hypoxia regulates cytoskeletal dynamics, we first sought hypoxia-induced and cytoskeleton-associated proteins. According to past microarray studies in glioblastoma [9–11] and the ELM database analysis [21], we predicted cyclin G2 as a candidate (Figure W1, *A–D*). Cyclin G2 expression was commonly upregulated among three subsets of microarray data in hypoxia-treated glioblastoma or hypoxic region of GBM, and it was positively correlated with hypoxia signature (hypoxia-responsive genes, e.g., *ANGPTL4* and *HK2*) [22,23] also in the other array data set (Figure W1, *B* and *C*); the ELM program predicted that cyclin G2 had a putative SH2 domain–binding motif in the N terminus, an actin-interacting WH2 motif, and an SH3 domain–binding motif in the C terminus (Figure W1*D*). In fact, cyclin G2 expression was significantly increased in glioblastoma-derived cell lines in response to hypoxic stimulations (Figure 1, *A* and *B*). In the human *ccng2* (which encodes cyclin G2 protein) promoter region, we found some putative hypoxia-responsive elements (HREs; -CGTG-; Figure W2) [24]. Through luciferase reporter assays using the human *ccng2* promoter region and ChIP, we revealed that cyclin G2 expression was directly regulated by HIF-1α (Figure 1, *C* and *D*). Knockdown of HIF-1α by RNA interference caused a deficit of the hypoxia-induced cyclin G2 expression (Figure 1*E* and data not shown). Interestingly, p53, which affects the malignancy of glioblastoma, had no relationship to cyclin G2 expression (U87MG, $p53^{WT}$; U251MG, $p53^{Mut}$; LNZ308, $p53^{Null}$, respectively), and the forced expression of p53 had no effect on cyclin G2 expression (Figure W3*A*). In primary glioblastoma, we detected immunoreactive signals for cyclin G2 in the cytoplasm of glioma cells, not in inflammatory cells (CD68 positive), in hypoxic regions such as pseudopalisades, whereas no signal was observed in high cellularity/mitotic regions (Figures 1, *F–R*, and W4, *A–D*).

Cyclin G2 is an unconventional cyclin, which interacts with an active complex of PP2A and induces cell cycle arrest [12]. Recent studies indicated cyclin G2 to be involved in the progression of oral squamous cell carcinoma [14] and breast carcinoma [15,16]. In breast cancer, cyclin G2 was defined as a marker of suppression of invasion and metastasis under the control of TAp63, a well-known regulator of carcinoma expansion. However, the mechanism by which cyclin G2 determines cellular behavior is completely unclear. Importantly, cyclin G2 expression is enhanced by a variety of transcriptional molecules such as FoxO3a [25,26], Nodal-ALK4/7 [27], and HIF-1α (as shown in Figure 1), which are all known as key promoters of glioblastoma expansion. Combined with our findings

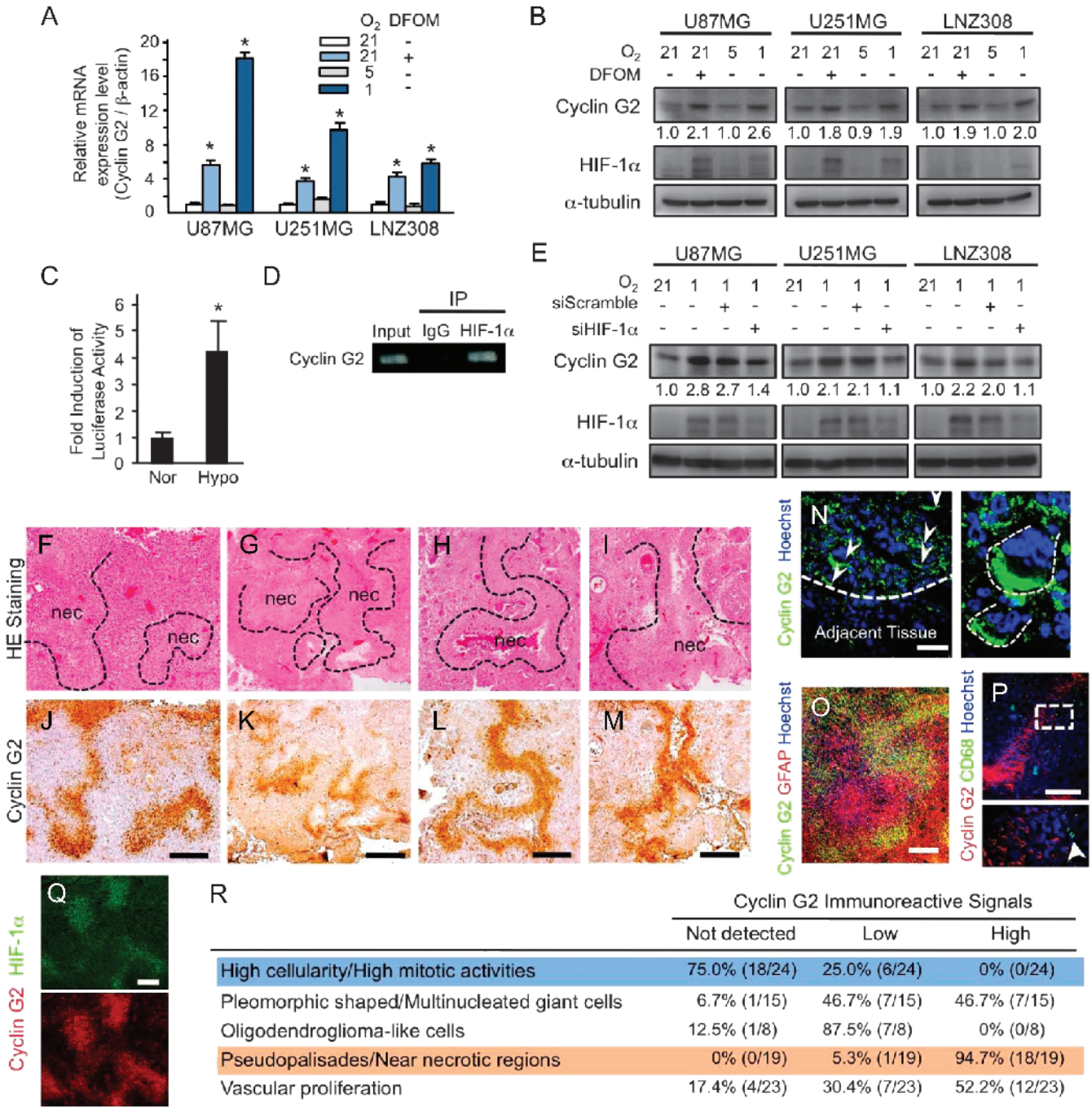

	Cyclin G2 Immunoreactive Signals		
	Not detected	Low	High
High cellularity/High mitotic activities	75.0% (18/24)	25.0% (6/24)	0% (0/24)
Pleomorphic shaped/Multinucleated giant cells	6.7% (1/15)	46.7% (7/15)	46.7% (7/15)
Oligodendroglioma-like cells	12.5% (1/8)	87.5% (7/8)	0% (0/8)
Pseudopalisades/Near necrotic regions	0% (0/19)	5.3% (1/19)	94.7% (18/19)
Vascular proliferation	17.4% (4/23)	30.4% (7/23)	52.2% (12/23)

Figure 1. Cyclin G2 is a hypoxia-induced protein and abundant in pseudopalisade-forming glioma cells. (A and B) Hypoxic conditions enhance *ccng2* mRNA transcription (A) and cyclin G2 protein expression (B). Cells were cultured in normoxic, deferoxamine mesylate (a reagent to mimic hypoxia)–added, or hypoxic conditions for 24 hours and subjected to reverse transcription–PCR or Western blot analysis. (C) Luciferase reporter assay with the human *ccng2* promoter/pGL4.14 vector. U87MG cells were transfected with the reporter vector and cultured in normoxic or hypoxic conditions for 24 hours. Bars represent the SD. (D) ChIP assay showing that cyclin G2 expression is directly regulated by HIF-1α. (E) Cyclin G2 expression is dependent on HIF-1α accumulation. Cells treated with siRNA against HIF-1α show lower expression of cyclin G2 than scrambled siRNA-treated cells under hypoxic conditions. (F–M) Human glioblastoma specimens stained with hematoxylin and eosin (H&E) and immunostained with anti–cyclin G2 antibody. Other images are shown in Figure W4. (N) Cyclin G2 accumulates at the leading edge of glioma cells migrating from the necrotic foci to adjacent tissue. (O and P) Cyclin G2 is abundant in pseudopalisade-forming glioma cells (O) but not in inflammatory cells (CD68 positive) (P). (Q and R) Cyclin G2 expression is abundant in hypoxic or near necrotic regions. Dotted lines indicate the borders of pseudopalisades (F–I). The scale bars represent 200 μm (J–M), 50 μm (N), 100 μm (O and P), respectively. Numbers in B and E represent the ratio of densitometry analysis.

that cyclin G2 is abundantly expressed in pseudopalisades, which consist of actively migrating glioma cells [4,5], we assumed that cyclin G2 had promotive effects on tumor expansion in glioblastoma, especially the hypoxia-driven local invasion, unlikely breast cancer.

Cyclin G2 Promotes GBM Migration

To test our hypothesis, we first investigated the role of cyclin G2 in the motility of glioblastoma cells. Wound-healing assays showed that hypoxia promoted the migration of glioblastoma cells (Figure 2*A*). As expected, the ectopically expressed cyclin G2 promoted migration of U87MG and U251MG cells even under normoxic conditions (Figure 2, *B*–*E*). To confirm this, we prepared cyclin G2–reduced U87MG and U251MG cells using a retroviral vector encoding shRNA against human *ccng2* (Figure 2*F*). The reduction in cyclin G2 caused excessive cell proliferation and p21 suppression, maybe because of the lack of cell cycle–inhibiting potential of cyclin G2 (Figure W3, *B* and *C*). Moreover, the shRNA-treated U87MG cells were flat and epithelia-like, unlike the spindle-shaped control cells (Figure 2*G*). Through wound-healing assays and single-cell tracing, we found that reduced expression of cyclin G2 caused the decrease in migration and cellular motility (Figure 2, *H*–*J*). In past studies, antiangiogenic treatment promoted the local invasion of glioblastoma cells by inducing hypoxic conditions [8]. According to our findings, cyclin G2 was involved in this. To verify this assumption, we intracranially implanted shRNA-treated U251MG cells into immunodeficient mice and treated them with CBO-P11, a vascular endothelial growth factor inhibitor. As previously reported [28], CBO-P11 reduced the cell density of the tumor core but promoted the local invasion of the cells treated with scrambled shRNA (Figure 2, *K*–*P*). In contrast, in cyclin G2–reduced U251MG cells, the local

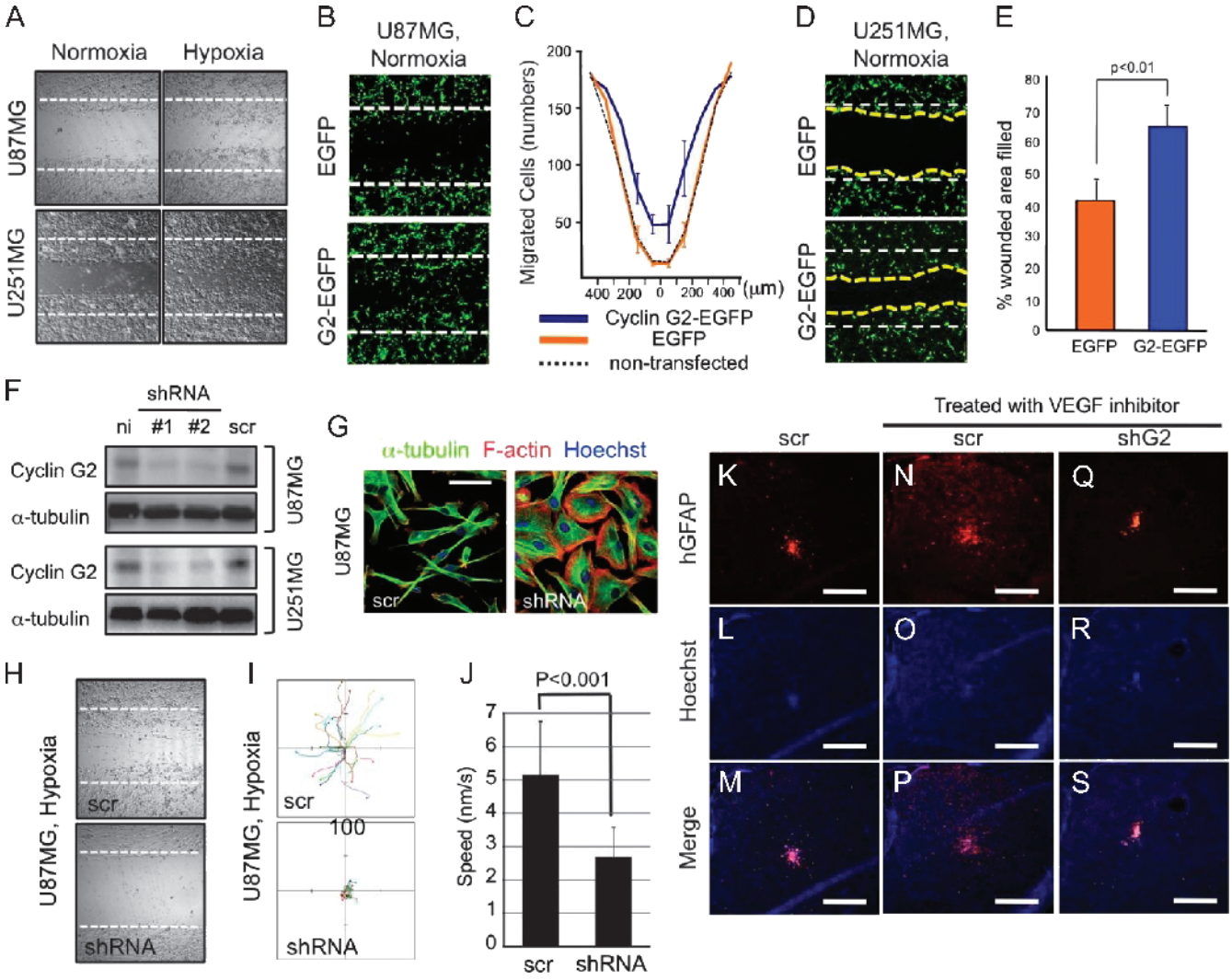

Figure 2. Cyclin G2 promotes glioblastoma cell migration and is required for the hypoxia-driven invasion of glioblastoma. (A) Hypoxia promotes the migration of glioma cells. (B–E) Wound-healing assay showing that forced expression of cyclin G2 promotes the migration even under normoxic conditions. The histograms show the number of EGFP-positive migrating cells in cyclin G2–EGFP– or EGFP-transfected U87MG cells (C) or the filled wounded area in U251MG cells (E). (F) U87MG and U251MG cells were infected with retroviral vectors encoding shRNA against human *ccng2* or scrambled shRNA. (G) A reduction in cyclin G2 expression changes the cell shape from spindle to flat in U87MG cells. (H–J) Knockdown of cyclin G2 results in reduced wound healing (H) and cellular motility (I). Motile speed is reduced by almost half (J). (K–S) Antiangiogenic treatment promotes the local invasion of glioblastoma cells in a cyclin G2–dependent manner. U251MG cells treated with shRNA against *ccng2* did not show migration induced by CBO-P11 treatment. The scale bars represent 20 μm (G) or 500 μm (K–S).

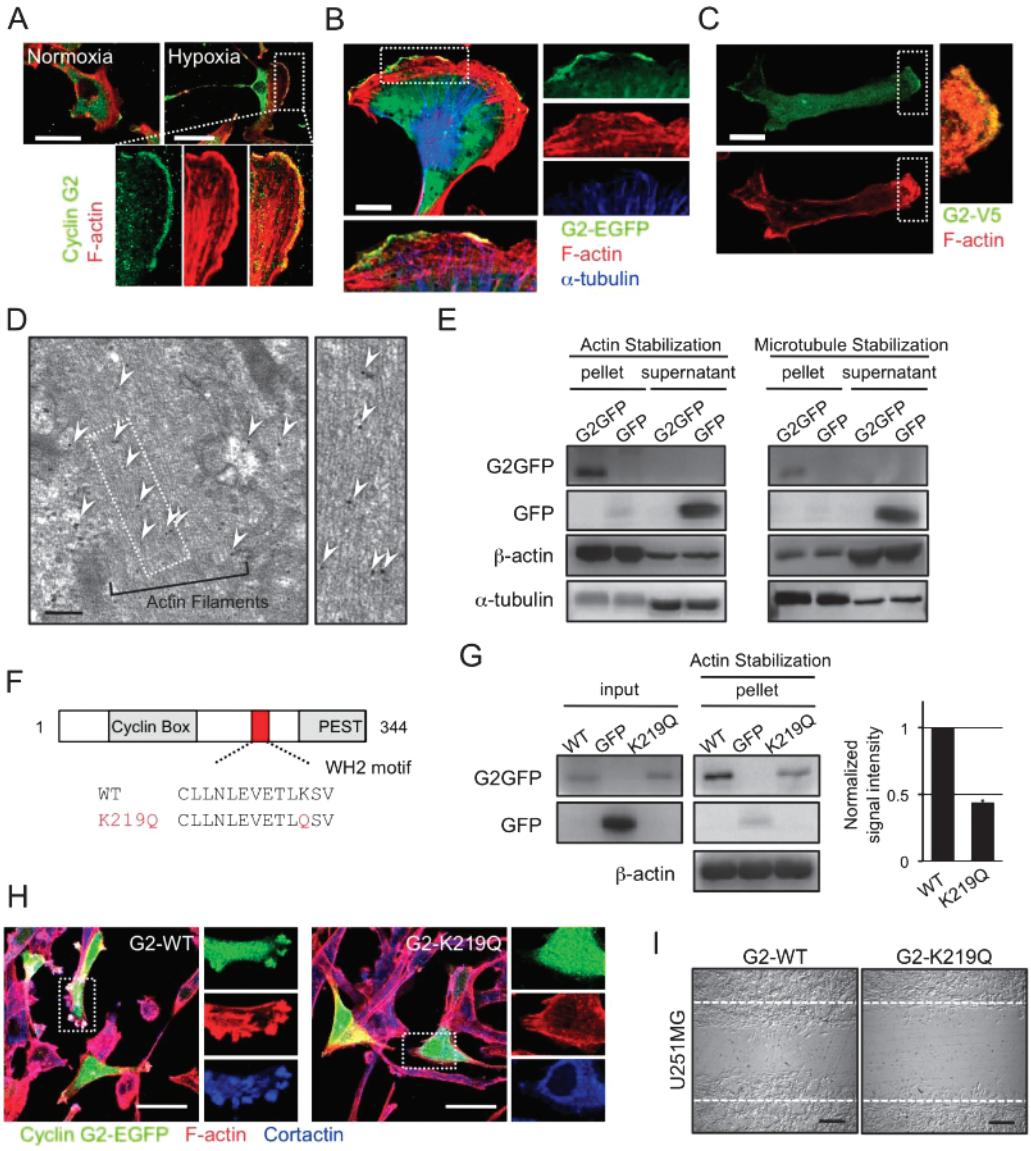

Figure 3. Cyclin G2 interacts with actin filaments, and the interaction is required for the motility of glioblastoma cells. (A) Endogenous cyclin G2 (green) localizes at the leading edge of migrating U87MG cells merging with F-actin (red). In hypoxia-stimulated U87MG cells, endogenous cyclin G2 accumulated at membrane ruffles. (B and C) Exogenously expressed cyclin G2–EGFP (B) and cyclin G2–V5 (C) also localize at the ruffles. (D) Immunoelectron microscopy of U87MG cells transfected with cyclin G2–EGFP. Arrowheads indicate the immunogold labeling of EGFP. (E) Cyclin G2 interacts with both filamentous actin and microtubules. (F) Cyclin G2 has a putative WH2 motif. (G–I) The K219Q mutant impairs the interaction with actin filaments (G), the potentiation of ruffle formation (H), and the consequent migration (I). Cortactin (blue) served as a marker of membrane ruffles (H). The scale bars represent 50 μm (A, H), 10 μm (B, C), 200 nm (D), or 200 μm (I).

invasion did not emerge (Figure 2, *Q*–*S*). These findings show that cyclin G2 is involved in the hypoxia-driven local invasion of glioblastoma.

Cyclin G2 Is a Cytoskeleton-Associated Protein

To examine the molecular mechanism of the cyclin G2–dependent tumor expansion, we next performed immunofluorescent analyses to detect the distribution of endogenous and exogenous cyclin G2 in glioma cells. Cyclin G2 occurred in the cytoplasm of U87MG cells in a normoxic and steady state (Figure 3*A*). However, under hypoxic conditions, the endogenous cyclin G2 accumulated at the leading edge, often referred to as membrane ruffles, merging with actin filaments (Figure 3*A*). The exogenously expressed cyclin G2–EGFP or cyclin G2–V5 also showed a peripheral distribution even under normoxic conditions (Figure 3, *B* and *C*). Immunoelectron microscopic analysis confirmed the co-localization of cyclin G2 and actin filaments (Figure 3*D*). In a previous study, cyclin G2 was shown to interact with microtubules [13]. To further understand the association between cyclin G2 and the cytoskeleton, we prepared a cytoskeletal pellet mainly containing actin filaments or microtubules (for details, see Materials and Methods section). Intriguingly, cyclin G2 was observed in the pellet under both actin-stabilizing (phalloidin and nocodazole treatment) and microtubule-stabilizing (latrunculin B and paclitaxel treatment) conditions (Figure 3*E*). On the basis of the ELM database prediction, cyclin G2 has a putative, actin-interacting WH2 motif (Figure 3*F*). To check whether cyclin G2 interacts with

actin filaments through this motif and affects actin polymerization, we prepared a K219Q mutant, which lacks the essential lysine in the WH2 motif [29]. In the actin-stabilized pellet, we observed a decreased signal of the K219Q mutant compared to wild-type cyclin G2, but total amounts of actin signals in the pellet seemed to be unchanged (Figure 3*G*). Moreover, the K219Q mutant lacks the potentiation of cyclin G2–induced ruffle formation and migration (Figure 3, *H* and *I*). These findings suggested that cyclin G2 interacted with actin filaments and affected the cytoskeletal dynamics at the leading edge of migrating cells using a certain mechanism, not promoting actin polymerization.

Cyclin G2 Promotes the Restricted Tyrosine Phosphorylation of Cortactin

We investigated the possibility that cyclin G2 might interact with cortactin and dynamin 2, actin-binding proteins and targets of oncogene src kinases [30], because they are well-defined regulators of actin dynamics and facilitators of ruffle formation, invadopodia formation, and consequent tumor invasion [31–33]. In glioblastoma cells, cyclin G2 co-localized with actin filaments and cortactin, or dynamin 2 at ruffles (Figure 4, *A* and *B*), and interacts with endogenous cortactin and dynamin 2 (Figure 4*C*). Notably, cyclin G2's reduction impaired cortactin's recruitment to the juxtamembrane and ruffle formation triggered by hypoxia (Figure 4, *D* and *E*), not by affecting cortactin expression levels (Figure 4*F*). These observations led to a hypothesis that enhanced expression of cyclin G2 owing to hypoxia or exogenous treatment influences actin dynamics and cellular motility by regulating cortactin or dynamin 2 function. In the regulation of actin dynamics in which cortactin and dynamin 2 are involved, tyrosine phosphorylation of cortactin is essential [34], and SFKs are required for the phosphorylation and consequent invasion [35]. Therefore, we investigated cortactin or dynamin 2 phosphorylation by immunoprecipitation and immunoblot analysis. In hypoxia-treated U87MG cells, cortactin, but not dynamin 2, was tyrosine-phosphorylated in an SFK-dependent manner (Figure 4*G*). This phosphorylation was also observed in hypoxic regions, typically pseudopalisades in glioblastoma specimens (Figure 4*H*), and seemed to be related to the abundance of cyclin G2 (Figure 4*I*). Surprisingly, even under normoxic conditions, the exogenously expressed cyclin G2 (tagged with EGFP or V5) also induced cortactin phosphorylation in an SFK-dependent manner (Figure 4, *J* and *K*). Elevated levels of cyclin G2 did not increase the total amount of tyrosine-phosphorylated protein (Figure W5*A*). These results show that abundant cyclin G2 induces the restricted tyrosine phosphorylation of cortactin. This could be explained by the fact that cyclin G2 was required for the localization of cortactin to the juxtamembrane, where SFKs phosphorylated cortactin. Ectopic cyclin G2 enhances the peripheral signal of phosphotyrosine in an SFK-dependent manner (Figure W5*B*). Furthermore, the increased motility by exogenous cyclin G2 as observed in Figure 2, *B* to *E*, was blocked by dasatinib but not erlotinib (Figure 4*L*). Although cyclin G2 binds to an active PP2A complex, the tyrosine phosphorylation of cortactin induced by abundant cyclin G2 was not influenced by okadaic acid (PP2A inhibitor) or D-*erythro*-S (PP2A activator) treatment (Figure 4*M*).

Cyclin G2 Is an SH3 Domain–Containing Protein that Provides a Functional Connection of Src, Cortactin, and Actin Cytoskeleton at the Ruffles

In primary glioblastoma, SFK expression was enhanced in the glioma cells that also expressed cyclin G2 abundantly (Figure 5*A*). In U87MG cells, hypoxic conditions enhanced, whereas ectopic cyclin G2 did not induce, the expression of fyn and src, which are effectors of oncogenic epidermal growth factor receptor signals in glioblastoma [36] (Figures 5*B* and W5*C*). These observations support our findings above that cyclin G2 promotes cortactin phosphorylation and consequent migration in concert with SFKs, and it may be appropriate to presume that the hypoxia-induced, excessive expression of cyclin G2 and SFKs synergistically potentiates the hypoxia-driven local invasion through the restricted tyrosine phosphorylation of cortactin.

Next, we examined the biochemical interaction between cyclin G2, cortactin, and SFKs. These proteins were co-immunoprecipitated (Figure 5*C*). According to the ELM-based prediction that cyclin G2 has a putative SH2 domain–binding motif and a noncanonical SH3 domain–binding motif (Figure 5*D*), we expected the N terminus of cyclin G2 to be important for cyclin G2–SFK interactions and the C terminus for cortactin phosphorylation. SH2 domain–containing proteins such as SFKs target phosphotyrosine-containing peptides in a sequence-specific manner [37]. As expected, we found that cyclin G2 was tyrosine-phosphorylated in an SFK-dependent manner (Figure 5*E*) and deletion of the N terminus in cyclin G2 (ΔN-G2) impaired cyclin G2–Src interaction (Figure 5*F*). A past study showed that a noncanonical SH3 domain–binding motif (PxxPxxP) was important for interaction with an SH3 domain–containing protein, cortactin [38]. The G2-P291A mutant ($G2^{P291A}$, which has a critical mutation in a noncanonical SH3 domain–binding motif) showed no interaction with cortactin and the consequent induction of tyrosine phosphorylation of cortactin and migration (Figures 5, *G* and *H*, and W5*D*). The $G2^{P291A}$ mutant did not cause ruffle formation and the recruitment of cortactin to the juxtamembrane in U87MG cells (Figure 5, *I*–*N*). Furthermore, to evaluate the effect of dasatinib on the tumor expansion induced by antiangiogenic treatment, we intracranially implanted U251MG cells and treated them with CBO-P11 alone or CBO-P11 plus dasatinib. As expected, dasatinib efficiently inhibited the expansion of glioma cells induced by CBO-P11 treatment (Figure 5, *O*–*T*). Combined with the results in Figure 2, *K* to *S*, these findings showed that the cyclin G2–SFKs–cortactin axis was required for the local invasion induced by hypoxia or antiangiogenic treatment *in vitro* and *in vivo* and the inhibition of SFKs by dasatinib attenuated it and that cyclin G2 acted upstream of SFK-cortactin.

Discussion

In summary, we demonstrated that cyclin G2 played pivotal roles in the regulation of actin dynamics in the hypoxia-driven local invasion of glioblastoma cells (Figure 5*U*). Severe hypoxia enhanced the expression of cyclin G2 and SFKs and the consequent formation of ruffles and cell migration by modulating the tyrosine phosphorylation of cortactin. Cyclin G2 orchestrates the recruitment to the juxtamembrane and SFK-dependent tyrosine phosphorylation of cortactin and thereby actin dynamics. We revealed that the SH2 or SH3 domain–binding motif and WH2 motif in cyclin G2 were important for this mechanism. Furthermore, we also found that cyclin G2 was a target of SFKs and phospho-cyclin G2 seemed to prefer the actin interaction. These findings provide the first evidence that cyclin G2 is a key regulator in the hypoxia-driven migration of glioblastoma cells. We are now investigating the relationship between cyclin G2 and other regulators of actin dynamics such as cdc42, rac1,

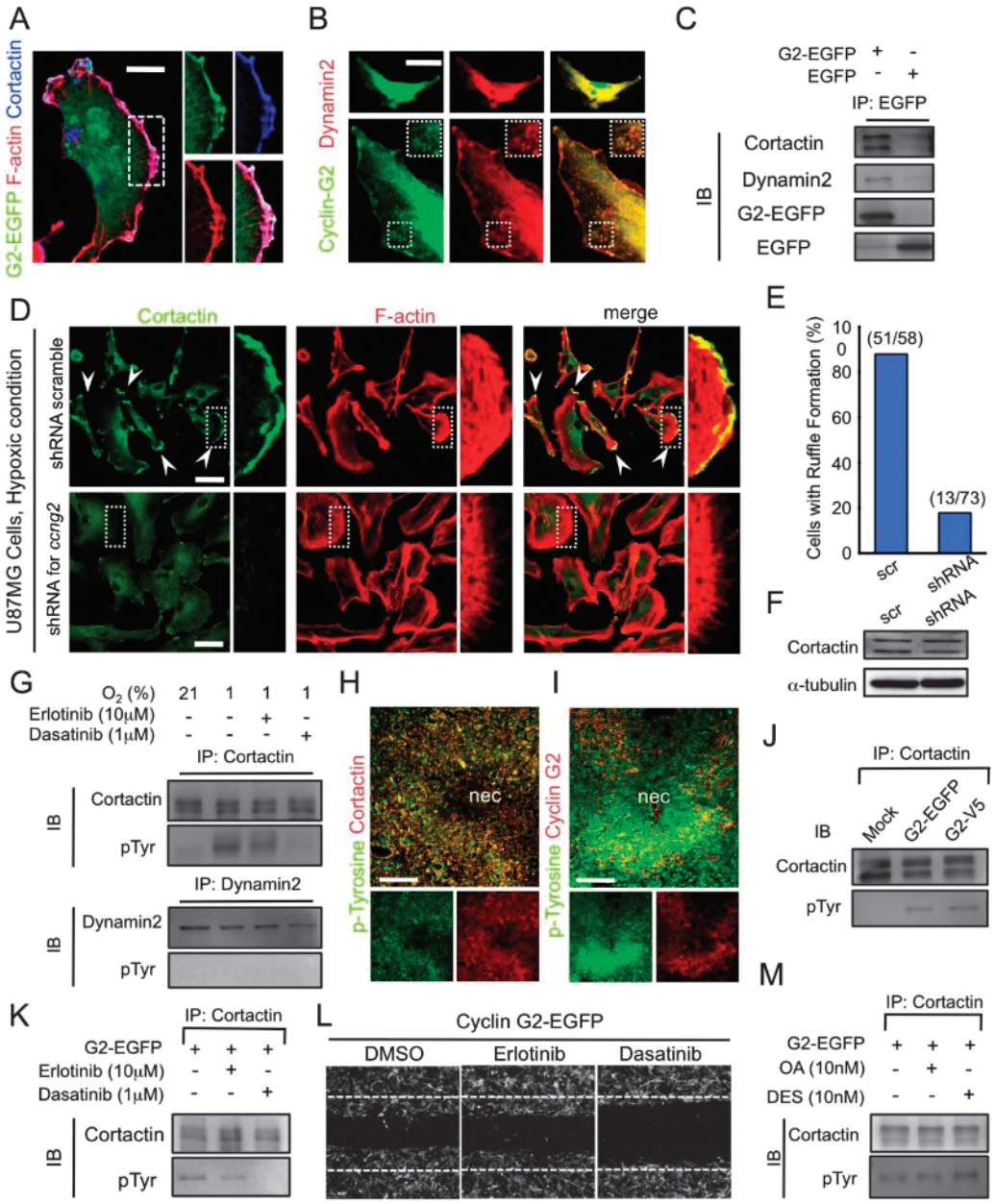

Figure 4. Cyclin G2 orchestrates cortactin tyrosine phosphorylation and the consequent migration of glioblastoma cells in concert with SFKs. (A and B) Cyclin G2 (green) co-localizes with F-actin (red) and cortactin (blue) (A), or dynamin 2 (B) at membrane ruffles. (C) Immunoprecipitation analysis shows that cyclin G2 interacts with endogenous cortactin and dynamin 2. (D–F) Cyclin G2 is required for the ruffle formation in response to hypoxia and the recruitment of cortactin to the juxtamembrane in glioblastoma cells (D). U87MG cells transfected with shRNA for human *ccng2* (lower panels) show fewer membrane ruffles than control cells (upper panels) in hypoxic conditions (E). Knockdown of cyclin G2 does not alter the expression level of cortactin (F). (G) Hypoxia induces tyrosine phosphorylation of cortactin, but not dynamin 2, in an SFK-dependent manner. (H and I) Phosphotyrosine signals are abundant near necrotic regions, merging with cortactin (H) and cyclin G2 (I). (J) Forced expression of cyclin G2 enhances the tyrosine phosphorylation of cortactin even under normoxic conditions. U87MG cells were transfected with cyclin G2–EGFP or cyclin G2–V5. (K) The tyrosine phosphorylation of cortactin induced by cyclin G2 is inhibited by dasatinib but not erlotinib. (L) Cyclin G2–enhanced wound healing is inhibited by dasatinib but not erlotinib. (M) PP2A activity seems to have no impact on the tyrosine phosphorylation. The scale bars represent 10 μm (A), 20 μm (B, D), or 200 μm (H, I).

and rhoA and the possibility that cyclin G2 affects signal transduction in which tyrosine phosphorylation is essential.

Concerning the therapeutic strategy for glioblastoma expansion, inhibiting the hypoxia-driven local invasion is imperative. According to our findings, decreasing the level of cyclin G2 is sufficient to inhibit the invasion (Figure 2, *K*–*S*). However, the reduction results in excessive proliferation because cyclin G2 acts as a negative regulator of the cell cycle (Figure W3, *B* and *C*). In the mechanism of the local invasion in which cyclin G2–SFKs–cortactin axis is involved, inhibiting SFKs is effective both *in vitro* and *in vivo*, in various cells including glioma-initiating cells (Figures 4, 5, and W6). Recent studies showing that SFKs such as fyn and src are ideal targets for glioblastoma expansion [35,36] support our observations.

Exactly why cyclin G2 determines cell behavior according to tumor origins remains unclear. As mentioned, cyclin G2 expression is enhanced by Nodal, a member of the transforming growth factor β superfamily. Interestingly, Nodal was recently identified as a facilitator of glioblastoma expansion [27], whereas it inhibits carcinoma expansion. Moreover, in breast carcinoma, p63, a master regulator of epithelial but not glial cell fate, is a key factor in the expression of cyclin G2, which is controlled by transforming growth factor β–Smad2 signaling [15]. Further studies are needed, but the different effects of cyclin G2 on tumor expansion may be because of signaling pathways that control carcinoma and glioma behavior.

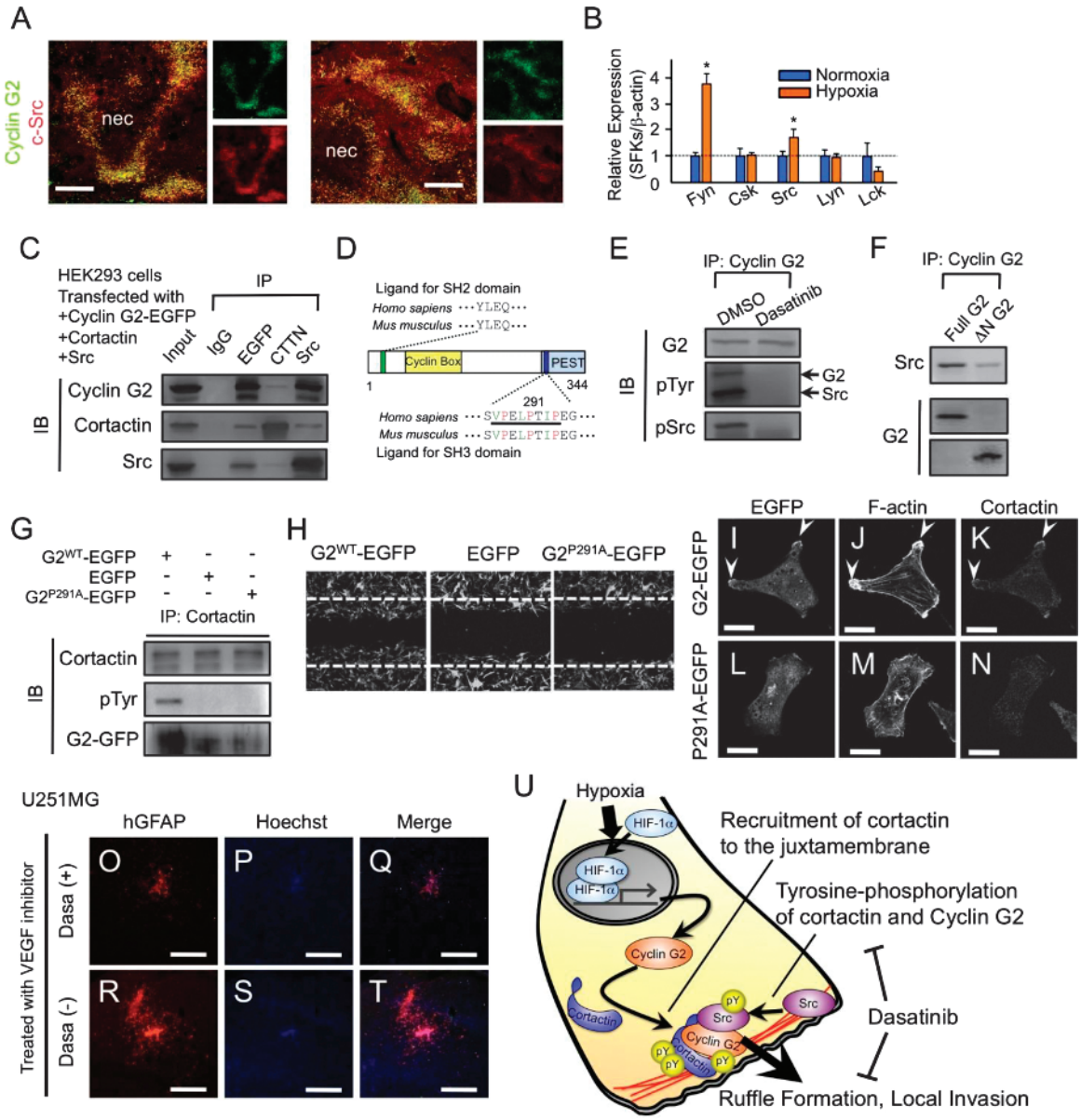

Figure 5. Molecular mechanism of the cyclin G2–driven tyrosine phosphorylation of cortactin and consequent invasion. (A) Immunofluorescent analysis showing that c-Src is abundantly expressed in pseudopalisades and most signals overlap with signals for cyclin G2. (B) Hypoxia significantly promotes the transcription of SFKs, Fyn, and Src in U87MG cells. (C) Cyclin G2, cortactin, and SFKs are co-immunoprecipitated. (D) Schematic diagram of the cyclin G2 protein. Cyclin G2 has a putative SH2 domain–binding motif at the N terminus and a noncanonical SH3 domain–binding motif (bar; 287-294) at the C terminus. Green letters indicate aliphatic amino acids (valine, leucine, and isoleucine), and red letters indicate proline. (E) Immunoprecipitation and immunodetections in HEK293 cells transfected with cyclin G2–EGFP and Src. Cyclin G2 is tyrosine-phosphorylated in an SFK-dependent manner. (F) Deletion of the N terminus (ΔN-G2) of cyclin G2 impairs the interaction with Src. (G and H) A single amino acid mutation (P291A) in the SH3 domain–binding motif of cyclin G2 ($G2^{P291A}$) impaired the induction of cortactin tyrosine phosphorylation (G) and consequent cell migration (H). (I–N) The P291A mutant impairs recruitment of cortactin to juxtamembrane. (O–T) Dasatinib inhibited the GBM expansion enhanced by anti–vascular endothelial growth factor treatment. (U) A model describing the role of cyclin G2 in the hypoxia-driven local invasion of glioblastoma cells. Cyclin G2 recruits cortactin to the leading edge of migrating glioma cells and promotes the consequent tyrosine phosphorylation of cortactin, which is essential for ruffle formation and tumor invasion. The scale bars represent 200 μm (A, O–T); "nec" indicates the necrotic foci in GBM specimens.

Acknowledgments

We thank Stefano Piccolo (Padova University) and Tomotoshi Marumoto (Kyushu University) for comments; Tomotoshi Marumoto, Hiroshi Yamada, and Koji Takei for gifts of materials; Hiroyuki Yanai and Takehiro Tanaka for pathologic assessment. We also thank Yumiko Morishita for the preparation of paraffin-embedded sections, Masumi Furutani for help with the electron microscopic study (Central Research Laboratory, Okayama University), and Ai Ueda for technical assistance in our laboratory (Okayama University).

References

[1] Wen PY and Kesari S (2008). Malignant gliomas in adults. *N Engl J Med* **359**, 492–507.

[2] Kaur B, Khwaja FW, Severson EA, Matheny SL, Brat DJ, and Van Meir EG (2005). Hypoxia and the hypoxia-inducible-factor pathway in glioma growth and angiogenesis. *Neuro Oncol* **7**, 134–153.

[3] Pàez-Ribes M, Allen E, Hudock J, Takeda T, Okuyama H, Viñals F, Inoue M, Bergers G, Hanahan D, and Casanovas O (2009). Antiangiogenic therapy elicits malignant progression of tumors to increased local invasion and distant metastasis. *Cancer Cell* **15**, 220–231.

[4] Rong Y, Durden DL, Van Meir EG, and Brat DJ (2006). 'Pseudopalisading' necrosis in glioblastoma: a familiar morphologic feature that links vascular pathology, hypoxia, and angiogenesis. *J Neuropathol Exp Neurol* **65**, 529–539.

[5] Brat DJ, Castellano-Sanchez AA, Hunter SB, Pecot M, Cohen C, Hammond EH, Devi SN, Kaur B, and Van Meir EG (2004). Pseudopalisades in glioblastoma are hypoxic, express extracellular matrix proteases, and are formed by an actively migrating cell population. *Cancer Res* **64**, 920–927.

[6] Ricci-Vitiani L, Pallini R, Biffoni M, Todaro M, Invernici G, Cenci T, Maira G, Parati EA, Stassi G, Larocca LM, et al. (2010). Tumour vascularization via endothelial differentiation of glioblastoma stem-like cells. *Nature* **468**, 824–828.

[7] Wang R, Chadalavada K, Wilshire J, Kowalik U, Hovinga KE, Geber A, Fligelman B, Leversha M, Brennan C, and Tabar V (2010). Glioblastoma stem-like cells give rise to tumour endothelium. *Nature* **468**, 829–833.

[8] Keunen O, Johansson M, Oudin A, Sanzey M, Rahim SA, Fack F, Thorsen F, Taxt T, Bartos M, Jirik R, et al. (2011). Anti-VEGF treatment reduces blood supply and increases tumor cell invasion in glioblastoma. *Proc Natl Acad Sci USA* **108**, 3749–3754.

[9] Méndez O, Zavadil J, Esencay M, Lukyanov Y, Santovasi D, Wang SC, Newcomb EW, and Zagzag D (2010). Knock down of HIF-1α in glioma cells reduces migration *in vitro* and invasion *in vivo* and impairs their ability to form tumor spheres. *Mol Cancer* **9**, 133.

[10] Marotta D, Karar J, Jenkins WT, Kumanova M, Jenkins KW, Tobias JW, Baldwin D, Hatzigeorgiou A, Alexiou P, Evans SM, et al. (2011). *In vivo* profiling of hypoxic gene expression in gliomas using the hypoxia marker EF5 and laser-capture microdissection. *Cancer Res* **71**, 779–789.

[11] Ragel BT, Couldwell WT, Gillespie DL, and Jensen RL (2007). Identification of hypoxia-induced genes in a malignant glioma cell line (U-251) by cDNA microarray analysis. *Neurosurg Rev* **30**, 181–187.

[12] Bennin DA, Don AS, Brake T, McKenzie JL, Rosenbaum H, Ortiz L, DePaoli-Roach AA, and Horne MC (2002). Cyclin G2 associates with protein phosphatase 2A catalytic and regulatory B′ subunits in active complexes and induces nuclear aberrations and a G_1/S phase cell cycle arrest. *J Biol Chem* **277**, 27449–27467.

[13] Arachchige Don AS, Dallapiazza RF, Bennin DA, Brake T, Cowan CE, and Horne MC (2006). Cyclin G2 is a centrosome-associated nucleocytoplasmic shuttling protein that influences microtubule stability and induces a p53-dependent cell cycle arrest. *Exp Cell Res* **312**, 4181–4204.

[14] Kim Y, Shintani S, Kohno Y, Zhang R, and Wong DT (2004). Cyclin G2 dysregulation in human oral cancer. *Cancer Res* **64**, 8980–8986.

[15] Adorno M, Cordenonsi M, Montagner M, Dupont S, Wong C, Hann B, Solari A, Bobisse S, Rondina MB, Guzzardo V, et al. (2009). A mutant-p53/Smad complex opposes p63 to empower TGFβ-induced metastasis. *Cell* **137**, 87–98.

[16] Montagner M, Enzo E, Forcato M, Zanconato F, Parenti A, Rampazzo E, Basso G, Leo G, Rosato A, Bicciato S, et al. (2012). SHARP1 suppresses breast cancer metastasis by promoting degradation of hypoxia-inducible factors. *Nature* **487**, 380–384.

[17] Marumoto T, Tashiro A, Friedmann-Morvinski D, Scadeng M, Soda Y, Gage FH, and Verma IM (2008). Development of a novel mouse glioma model using lentiviral vectors. *Nat Med* **15**, 110–116.

[18] Xu G, Bernaudo S, Fu G, Lee DY, Yang BB, and Peng C (2008). Cyclin G2 is degraded through the ubiquitin-proteasome pathway and mediates the anti-proliferative effect of activin receptor-like kinase 7. *Mol Biol Cell* **19**, 4968–4979.

[19] Aguilar V, Annicotte JS, Escote X, Vendrell J, Langin D, and Fajas L (2010). Cyclin G2 regulates adipogenesis through PPARγ coactivation. *Endocrinology* **151**, 5247–5254.

[20] Fujimura A, Michiue H, Nishiki T, Ohmori I, Wei FY, Matsui H, and Tomizawa K (2011). Expression of a constitutively active calcineurin encoded by an intron-retaining mRNA in follicular keratinocytes. *PLoS One* **6**, e17685.

[21] Puntervoll P, Linding R, Gemünd C, Chabanis-Davidson S, Mattingsdal M, Cameron S, Martin DM, Ausiello G, Brannetti B, Costantini A, et al. (2003). ELM server: a new resource for investigating short functional sites in modular eukaryotic proteins. *Nucleic Acids Res* **31**, 3625–3630.

[22] Kim SH, Park YY, Kim SW, Lee JS, Wang D, and DuBois RN (2011). ANGPTL4 induction by prostaglandin E_2 under hypoxic conditions promotes colorectal cancer progression. *Cancer Res* **71**, 7010–7020.

[23] Wolf A, Agnihotri S, Micallef J, Mukherjee J, Sabha N, Cairns R, Hawkins C, and Guha A (2011). Hexokinase 2 is a key mediator of aerobic glycolysis and promotes tumor growth in human glioblastoma multiforme. *J Exp Med* **208**, 313–326.

[24] Semenza GL, Jiang BH, Leung SW, Passantimo R, Concordet JP, Marie P, and Giallongo A (1996). Hypoxia response elements in the aldolase A, enolase 1, and lactate dehydrogenase A gene promoters contain essential binding sites for hypoxia-inducible factor 1. *J Biol Chem* **271**, 32529–32537.

[25] Martínez-Gac L, Marqués M, García Z, Campanero MR, and Carrera AC (2004). Control of cyclin G2 mRNA expression by forkhead transcription factors: novel mechanism for cell cycle control by phosphoinositide 3-kinase and forkhead. *Mol Cell Biol* **24**, 2181–2189.

[26] Fu G and Peng C (2011). Nodal enhances the activity of FoxO3a and its synergistic interaction with Smads to regulate cyclin G2 transcription in ovarian cancer cells. *Oncogene* **30**, 3953–3966.

[27] Lee CC, Jan HJ, Lai JH, Ma HI, Hueng DY, Lee YC, Cheng YY, Liu LW, Wei HW, and Lee HM (2010). Nodal promotes growth and invasion in human gliomas. *Oncogene* **29**, 3110–3123.

[28] Zilberberg L, Shinkaruk S, Lequin O, Rousseau B, Hagedorn M, Costa F, Caronzolo D, Balke M, Canron X, Convert O, et al. (2003). Structure and inhibitory effects on angiogenesis and tumor development of a new vascular endothelial growth inhibitor. *J Biol Chem* **278**, 35564–35573.

[29] Co C, Wong DT, Gierke S, Chang V, and Taunton J (2007). Mechanism of actin network attachment to moving membranes: barbed end capture by N-WASP WH2 domains. *Cell* **128**, 901–913.

[30] Singh VP and McNiven MA (2008). Src-mediated cortactin phosphorylation regulates actin localization and injurious blebbing in acinar cells. *Mol Biol Cell* **19**, 2339–2347.

[31] Feng H, Liu KW, Guo P, Zhang P, Cheng T, McNiven MA, Johnson GR, Hu B, and Cheng SY (2012). Dynamin 2 mediates PDGFRα-SHP-2-promoted glioblastoma growth and invasion. *Oncogene* **31**, 2691–2702.

[32] Oser M, Yamaguchi H, Mader CC, Bravo-Cordero JJ, Arias M, Chen X, Desmarais V, van Rheenen J, Koleske AJ, and Condeelis J (2009). Cortactin regulates cofilin and N-WASp activities to control the stages of invadopodium assembly and maturation. *J Cell Biol* **186**, 571–587.

[33] Mader CC, Oser M, Magalhaes MA, Bravo-Cordero JJ, Condeelis J, Koleske AJ, and Gil-Henn H (2011). An EGFR-Src-Arg-Cortactin pathway mediates functional maturation of invadopodia and breast cancer cell invasion. *Cancer Res* **71**, 1730–1741.

[34] Kruchten AE, Krueger EW, Wang Y, and McNiven MA (2008). Distinct phospho-forms of cortactin differentially regulate actin polymerization and focal adhesions. *Am J Physiol Cell Physiol* **295**, C1113–C1122.

[35] Lu KV, Zhu S, Cvrljevic A, Huang TT, Sarkaria S, Ahkavan D, Dang J, Dinca EB, Plaisier SB, Oderberg I, et al. (2009). Fyn and Src are effectors of oncogenic epidermal growth factor receptor signaling in glioblastoma patients. *Cancer Res* **69**, 6889–6898.

[36] Du J, Bernasconi P, Clauser KR, Mani DR, Finn SP, Beroukhim R, Burns M, Julian B, Peng XP, Hieronymus H, et al. (2009). Bead-based profiling of tyrosine kinase phosphorylation identifies SRC as a potential target for glioblastoma therapy. *Nat Biotechnol* **27**, 77–83.

[37] Liu BA, Jablonowski K, Raina M, Arcé M, Pawson T, and Nash PD (2006). The human and mouse complement of SH2 domain proteins—establishing the boundaries of phosphotyrosine signaling. *Mol Cell* **22**, 851–868.

[38] Tian L, Chen L, McClafferty H, Sailer CA, Ruth P, Knaus HG, and Shipston MJ (2006). A noncanonical SH3 domain binding motif links BK channels to the actin cytoskeleton via the SH3 adapter cortactin. *FASEB J* **20**, 2588–2590.

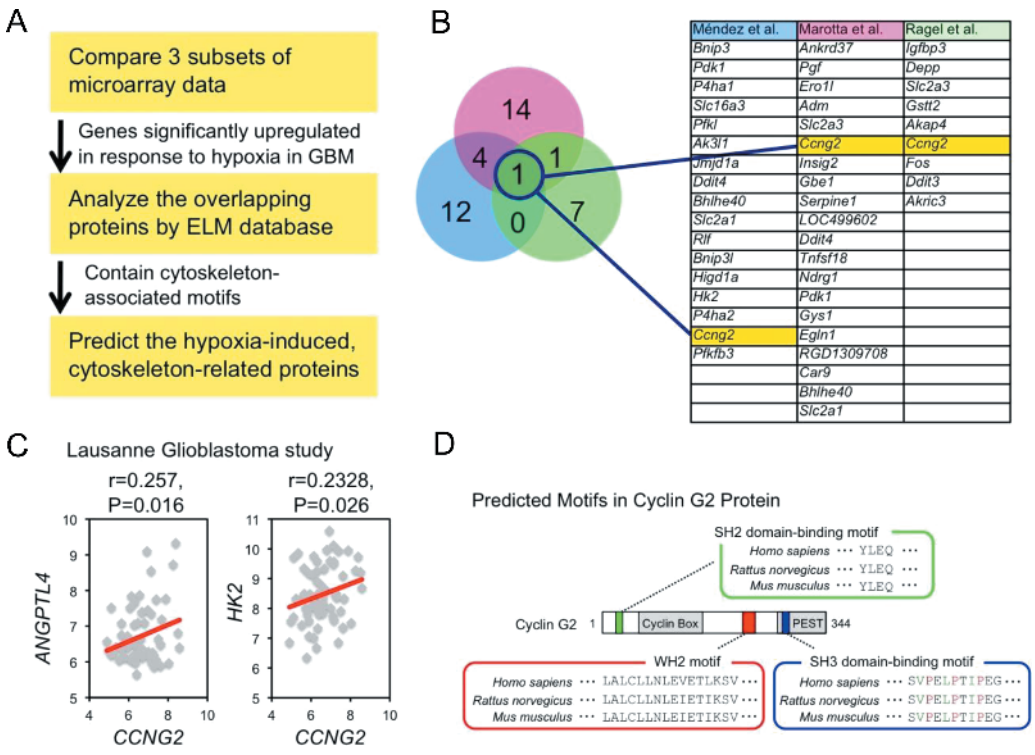

Figure W1. (A) Diagram of the procedure to predict the hypoxia-induced and cytoskeleton-associated proteins in human glioma cell lines. (B) *Cyclin G2* is a commonly upregulated gene in response to hypoxia among three subsets of microarray data of glioblastoma study. (C) The expression level of cyclin G2 is correlated with hypoxia-responsive genes, *ANGPTL4* and *HK2*, in Lausanne glioblastoma study (Accession ID: GSE7696). (D) The ELM database predicts that cyclin G2 protein has a putative SH2 or SH3 domain–binding motif and WH2 motif.

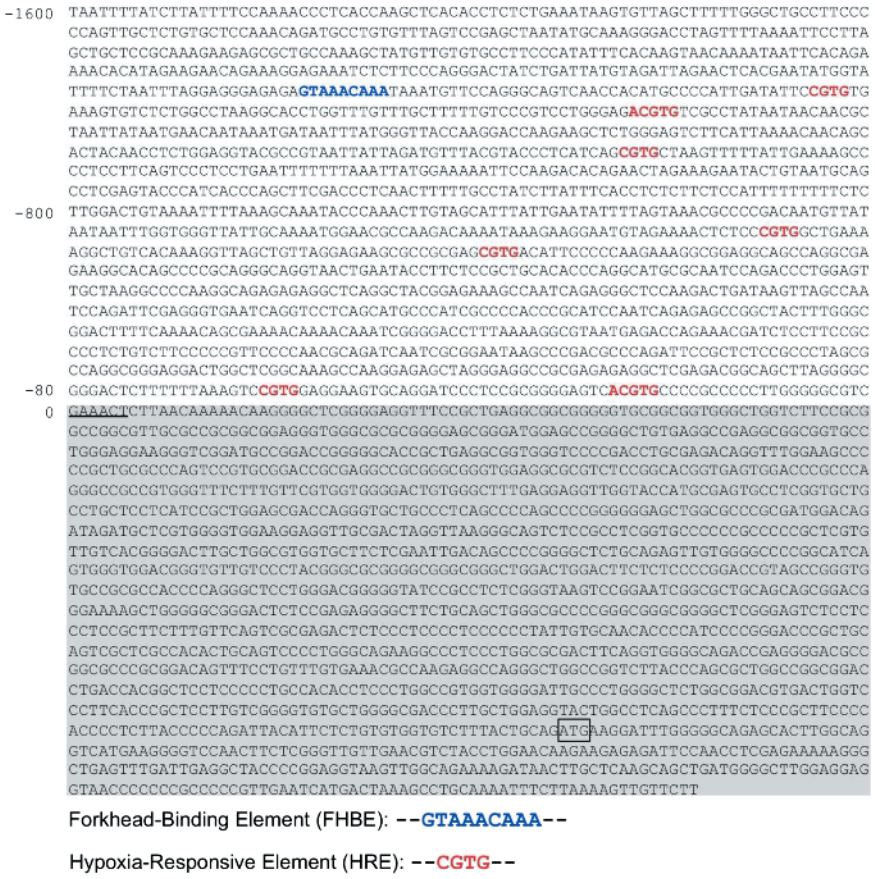

Figure W2. The human cyclin G2 promoter region contains putative HREs. The human cyclin G2 promoter region (−1600~0) contains some putative HREs (-CGTG-; red) and a FoxO3a-binding site (blue). The transcription starting site (underlined in shaded sequence) and the translation initiating ATG (boxed) were determined according to NCBI (Accession No. NM_004354.2).

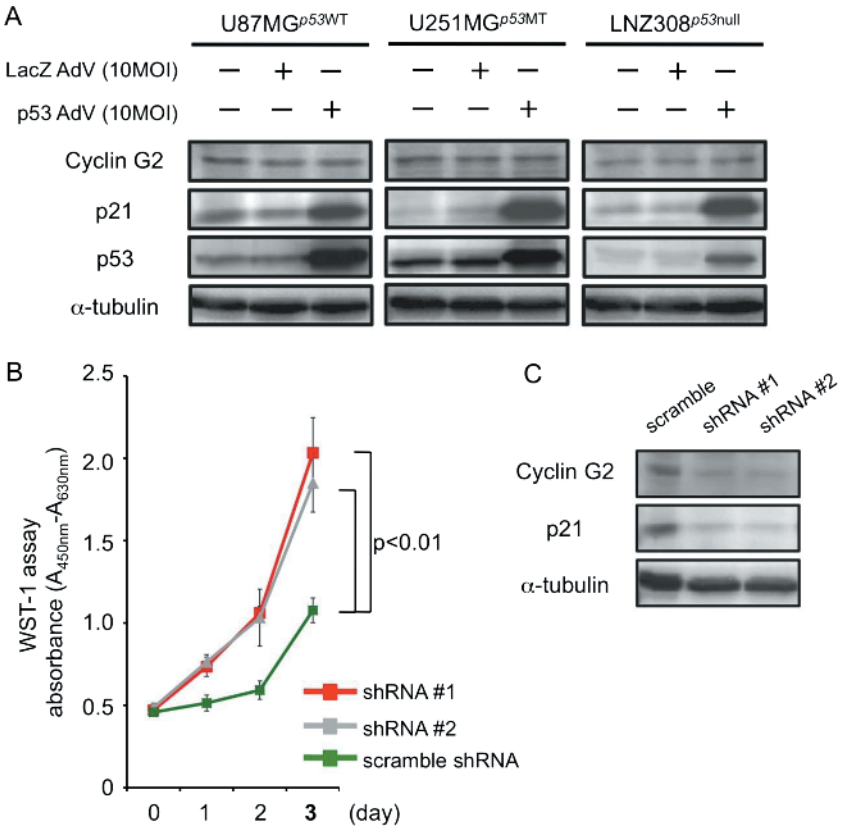

Figure W3. (A) Western blot analyses of U87MG (p53^{WT}), U251MG (p53^{Mut}), and LNZ308 (p53^{Null}) cells infected with *lacZ* or p53 adenovirus. These results show that the level of p53 does not affect that of cyclin G2 and forced expression of p53 does not induce cyclin G2 expression in GBM. (B) WST-1 assay showing the effect of cyclin G2's reduction on cell-cycle regulation in U87MG cells. (C) Cyclin G2 reduction resulted in p21 suppression.

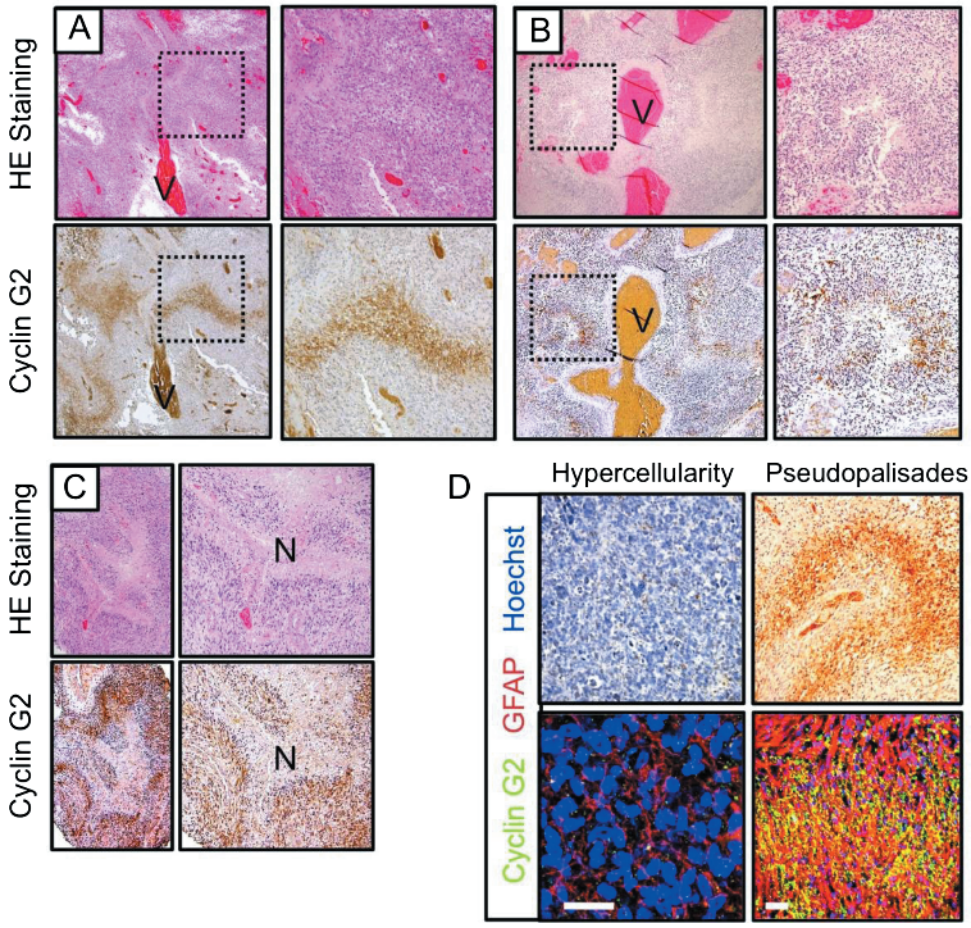

Figure W4. Cyclin G2 is abundant in pseudopalisade-forming glioma cells. (A–C) Cyclin G2 expression in pseudopalisades is observed in various types of GBM specimens. (D) Cyclin G2 is absent in high cellularity/high mitotic regions in GBM. The scale bars represent 10 μm in D. "V" and "N" indicate vessel and necrosis, respectively.

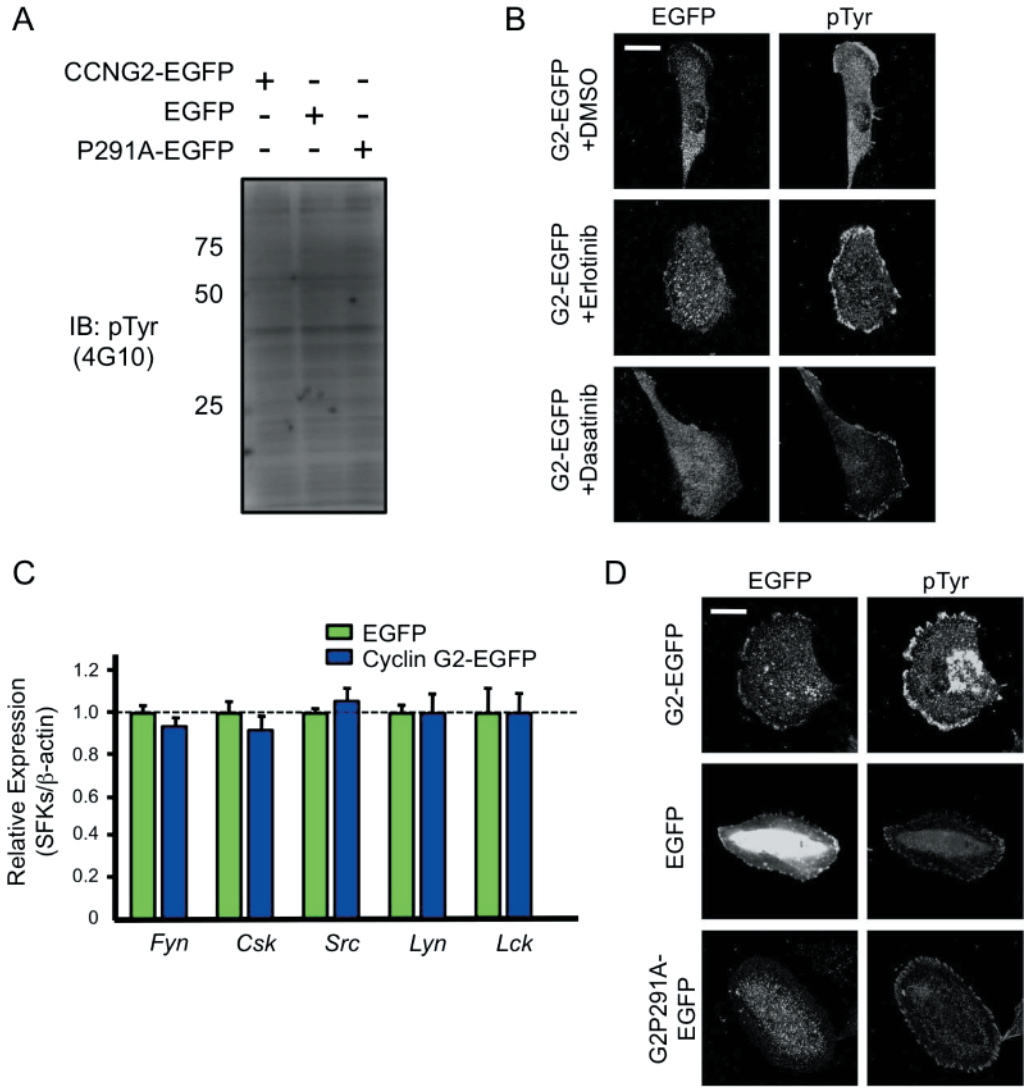

Figure W5. Cyclin G2 induces the restricted tyrosine phosphorylation of cortactin in an SFK-dependent manner. (A) Ectopic expression of cyclin G2 does not alter the total amount of tyrosine phosphorylation. (B) Dasatinib inhibits the phosphorylation induced by cyclin G2. Note that dasatinib, but not erlotinib, decreases the peripheral signals of phosphotyrosine induced by cyclin G2. The scale bar represents 10 μm in B. (C) Cyclin G2 does not enhance transcription of SFK mRNA. (D) Exogenous cyclin G2 increases, whereas the P291A mutant impairs, tyrosine phosphorylation signals at the juxtamembrane. The scale bar represents 10 μm in D.

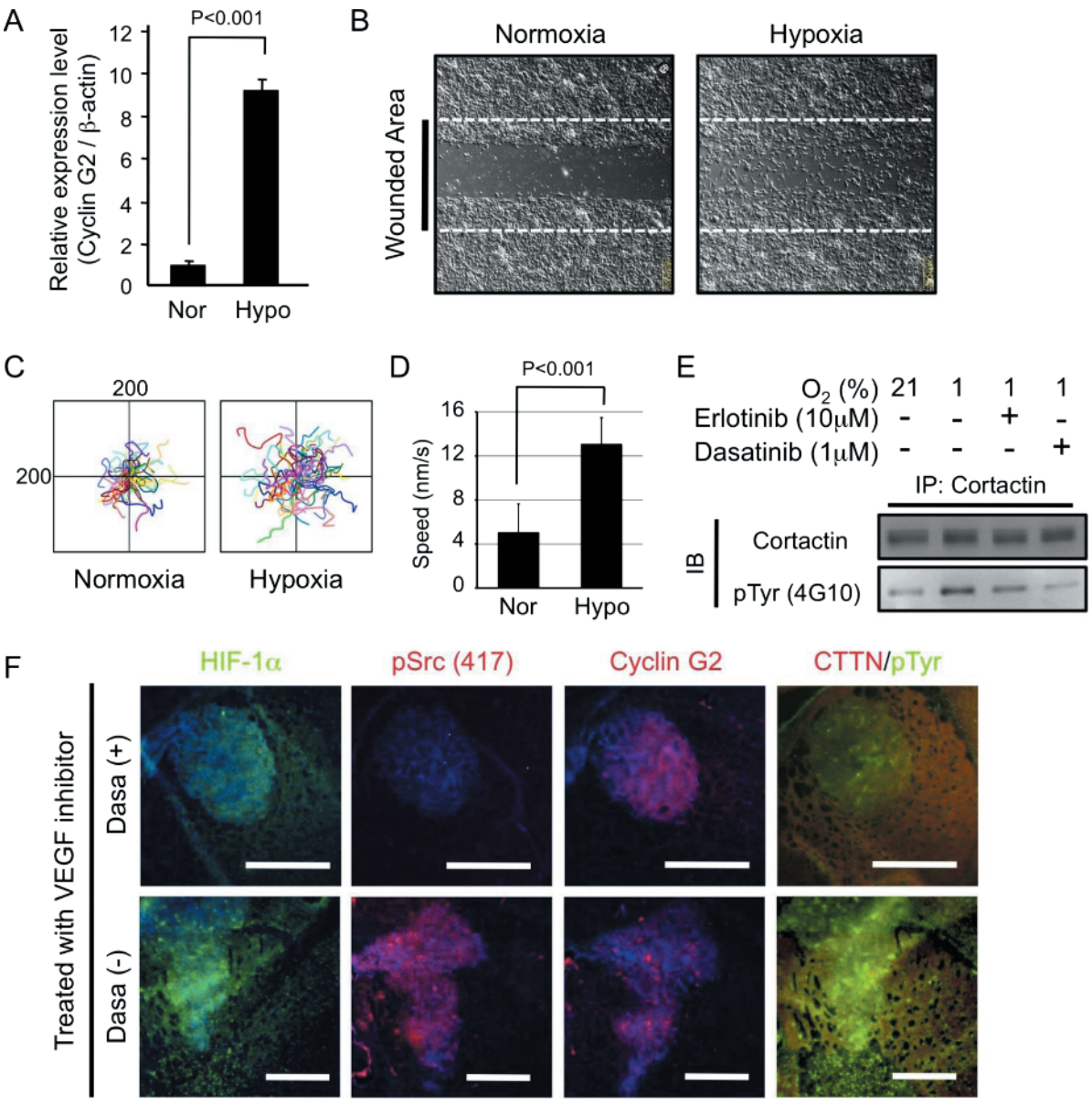

Figure W6. The effectiveness of dasatinib on the expansion of glioma-initiating cells. (A) Cyclin G2 expression is enhanced in response to hypoxia in murine glioma-initiating 005 cells. (B–D) Hypoxia stimulates the motility of 005 cells. (E) Tyrosine phosphorylation of cortactin is enhanced in response to hypoxic stimulation in 005 cells and dasatinib attenuates it. Note that 005 cells show the phosphorylation in a normoxic and steady state. (F) Dasatinib attenuates the hypoxia-driven local invasion of 005 cells. Note that dasatinib treatment inhibits the phosphorylation of src and cortactin. The scale bars represent 200 μm (F).

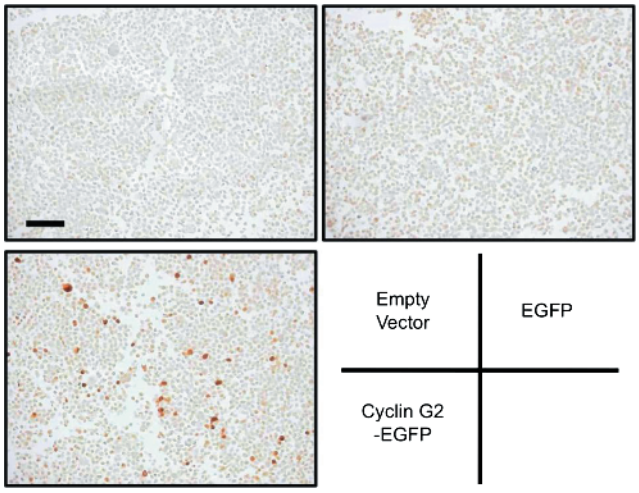

Figure W7. Goat anti-human cyclin G2 antibody (Santa Cruz Biotechnology, Inc) successfully recognized ectopic cyclin G2 in paraffin-embedded HEK293 cells that were transfected with cyclin G2–EGFP. For other applications including immunoblot analysis, see references. The scale bar represents 100 μm.

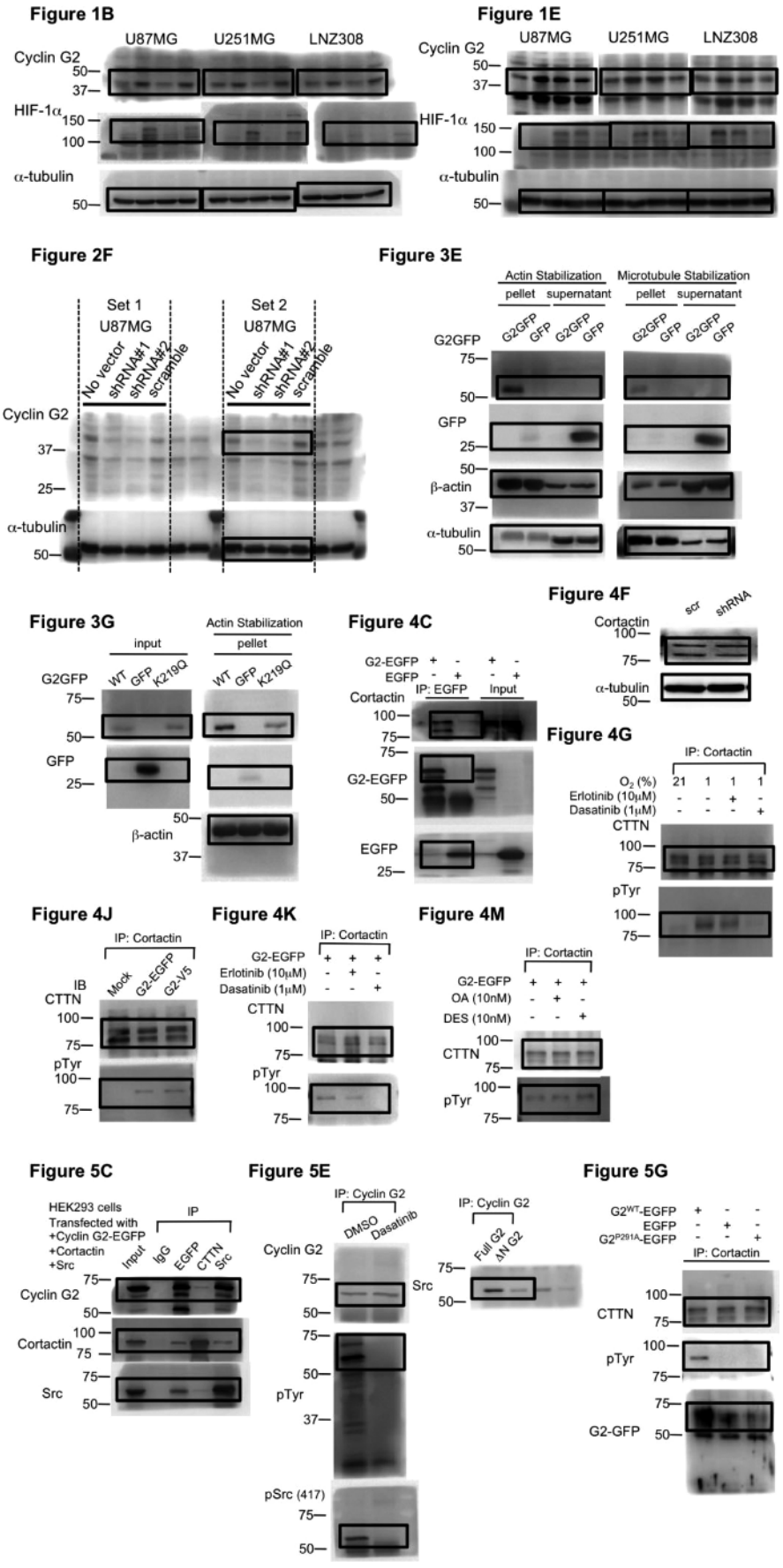

Figure W8. Full scans of the immunoblots shown in the figures. Boxes indicate the parts used in the figures, and numbers indicate the molecular weights. All data were obtained with the VersaDoc Imaging System (Bio-Rad).